MANUSCRIPT

Lanmodulin's EF 2-3 Domain: Insights from Infrared Spectroscopy and Simulations

Eman A. Alasadi[1,†], Wonseok Choi[2,†], Xiaobing Chen[1], Joseph A. Cotruvo, Jr.,[2,*] and Carlos R. Baiz[1,*]

[†]*Authors contributed equally*

[1]Department of Chemistry, University of Texas at Austin, 105 E 24th St. A5300, Austin, TX 78712, USA

[2]Department of Chemistry, The Pennsylvania State University, University Park, PA 16802, USA

*Corresponding authors: cbaiz@cm.utexas.edu and juc96@psu.edu

Keywords

Ultrafast Dynamics, Molecular Dynamics, Lanmodulin, EF Hand, Spectroscopy

Abstract

Lanmodulins are small, ~110-residue proteins with four EF-hand motifs that demonstrate picomolar affinity for lanthanide ions, making them efficient in the recovery and separation of these technologically important metals. In this study, we delve into the thermodynamic and structural complexities of lanthanide ion binding to a 41-residue domain, EF 2-3, that constitutes the two highest-affinity metal-binding sites in the lanmodulin protein from *Methylorubrum extorquens*. Using a combination of circular dichroism (CD) spectroscopy, isothermal titration calorimetry (ITC), two-dimensional infrared (2D IR) spectroscopy, and molecular dynamics (MD) simulations, we characterize the binding capabilities of EF 2-3. ITC demonstrates that binding is occurring between peptide and lanthanides with conditional dissociation constants (K_d) in the range of 20-30 μM, with no significant differences in the K_d values for La^{3+}, Eu^{3+}, and Tb^{3+} at pH 7.4. In addition, CD spectroscopy suggests that only one binding site of EF 2-3 undergoes a significant conformational change in the presence of lanthanides. 2D IR spectroscopy demonstrates the presence of both mono- and bidentate binding configurations in EF 2-3 with all three lanthanides. MD simulations, supported by Eu luminescence measurements, explore these results, suggesting a competition between water-lanthanide and carboxylate-lanthanide interactions in the EF 2-3 domain. These results underscore the role of the core helical bundle of the protein architecture in influencing binding affinities and communication between the metal-binding sites in the full protein.

1. Introduction

The elements of the lanthanide series, along with scandium and yttrium, are categorized as rare-earth elements (REEs). Although REEs are generally abundant in the Earth's crust, their similar physicochemical properties and thus co-occurrence with one another (as well as with other metals) make their mining, separation, and purification processes challenging.[1-4] Conventional methods require large solvent quantities and complex extraction processes and have significant environmental impacts.[5] Given that rare earth elements are crucial for emerging technologies, there is an escalating demand for more efficient and environmentally friendly separation techniques.

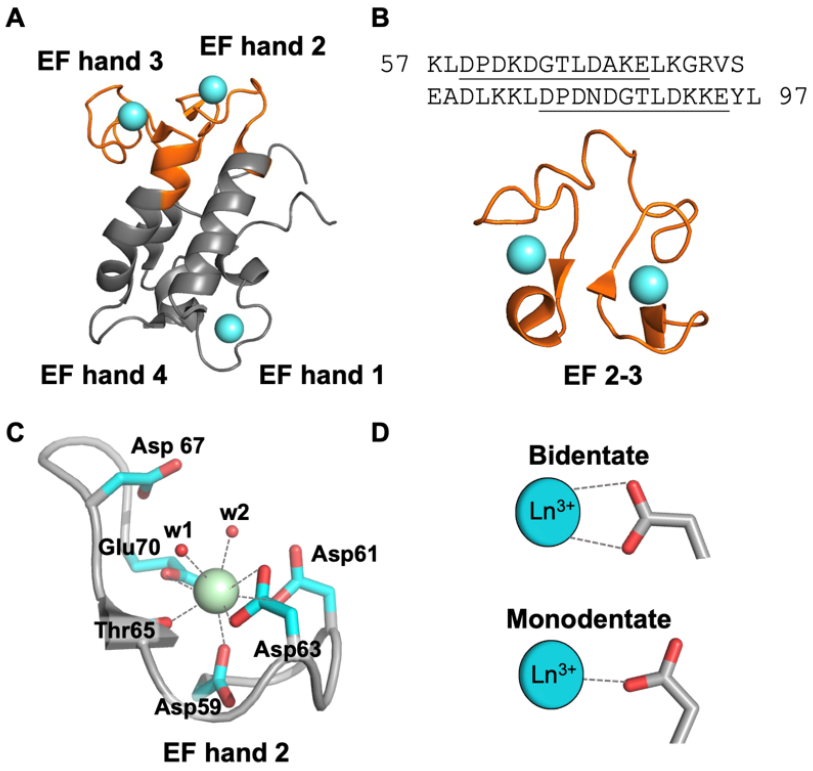

Figure 1. (A) NMR solution structure of yttrium-bound LanM (PDB: 6MI5).[6] LanM contains four EF hands, each flanked by two alpha helices. EF hands 1, 2, and 3 bind Y^{3+} ions, shown in cyan, with low-picomolar affinity (pH 7), whereas EF hand 4 remains unbound due to its lower binding affinity. The region encompassing the EF hand 2 and 3 peptide used in the present study is depicted in orange. (B) Top: Sequence of the unit connecting EF hands 2 and 3 (EF 2-3), with two additional amino acids at both the N- and C-termini included in the present studies. The sequences of EF hands 2 and 3 are underlined. Bottom: Top view of the truncated EF 2-3 from the NMR structure. (C) A detail of EF hand 2, obtained from the X-ray crystal structure of Nd^{3+}-bound LanM (PDB 8FNS).[7] D59, D61, and the carbonyl backbone of T65 are monodentate, while D63 and E70 are bidentate, completing 9-coordination with two water molecules (w1 and w2). (D) Schematic representation of binding geometries. Bidentate binding involves carboxylate oxygens directly interacting with the metal ion, whereas monodentate binding occurs when only one oxygen binds to the ion.

The recent discovery that biology utilizes certain lanthanides in essential functions[8, 9] provides a potential framework for the use of biological and/or biochemical processes to mitigate some of the challenges associated with recovering and separating rare earths. Lanmodulin (LanM), which was first identified and characterized in *Methylorubrum extorquens*, is a prototypal ligand for understanding selective REE binding in biology.[10] LanM possesses several features that make

it a promising tool for efficient rare earth element separation.[10] It features four carboxylic acid-rich EF-hands (denoted EF1 through EF4), three of which exhibit picomolar affinity and remarkable selectivity for lanthanides (**Figure 1A**), higher than even engineered EF-hands such as the lanthanide-binding tag.[11] For example, LanM preferentially binds lanthanides over metals such as $Fe^{2+/3+}$, Al^{3+}, Mn^{2+}, and Cu^{2+}.[12, 13] LanM exhibits 100-million-fold stronger affinity for lanthanides compared to calcium, the ligand for typical EF hands. In addition, LanM's high thermal stability and resilience in acidic conditions are beneficial for practical purposes.[12] With these remarkable features, LanM was highlighted in a proof-of-principle REE separation method where >99% purity was achieved in Nd/Dy separation within one or two steps, depending on feed composition.[13]

LanM is thought to achieve its high selectivity for REEs through the folding transition induced upon REE binding (and particularly for larger, light REEs like Nd^{3+}).[6, 10] Specifically, the metal-binding loop provides the optimized coordination sphere for REEs, e.g., a coordination number of 9 for Nd^{3+}, contrary to the coordination number of 7 for Ca^{2+} binding sites in canonical EF-hand proteins like calmodulin (CaM) (**Figure 1C**).[7, 14] The extensive hydrophobic interactions and hydrogen bonds between the three core helices are also thought to stabilize the protein's REE-induced folded state.[6] EF 2 and EF 3 first recognize the metal with high cooperativity and induce formation of roughly 2/3 of the alpha helical content of the fully folded protein.[15, 16] Nonetheless, the exact contributions of these structural elements to LanM's affinity and selectivity remain to be fully elucidated.

In this study, we seek to determine whether the unique binding properties of LanM can be preserved in a smaller domain. Initial biochemical[10, 15] and structural[6] studies indicated that individual EF hands would not be sufficient, and this conclusion was supported by a subsequent study of the 12-residue peptides of the 4 EF-hands.[17] As EF 2 and EF 3 in LanM have the highest binding affinities and evident cooperative interaction,[15] and as these EF hands seem to be most critical for performance of the protein in REE sensing and separation experiments[13, 15], we focus on EF 2 and EF 3 as interconnected motifs, using the 41-residue peptide that will be referred to as EF 2-3 (**Figure 1B)**. This peptide includes two additional amino acids from the original LanM at the N- and C-termini. We centered our observations on the interplay between ion size, affinity, and the binding geometry of EF 2-3 across three lanthanides: La^{3+}, Eu^{3+}, and Tb^{3+}. Utilizing protein domains may present a strategy for future separations. Evidently, for effective sequence design and application, it is necessary to understand the structure-affinity relationship in these systems.

Vibrational spectroscopy is an ideal tool to probe conformational changes upon lanthanide binding. Specifically, ultrafast two-dimensional infrared (2D IR) spectroscopy, uses a sequence of ultrashort pulses to probe ion-dependent structural changes of EF hand geometries.[18-20] Binding populations from the IR lineshapes can then be extracted using similar methods described previously.[19] The 2D IR measurements[18-20] are interpreted through molecular dynamics (MD) simulations[21-23], which produce an atomistic representation of the ion size and charge effects on coordination. In addition, we use isothermal titration calorimetry (ITC), and circular dichroism (CD) spectroscopy, to measure binding stoichiometries and affinities. Together, our results indicate the importance of communication between the two EF-hands and yet also that these two EF-hands alone are insufficient to reproduce the affinity and selectivity of the full-length protein.

2. Methods

a. <u>EF Hand 2-3 Peptide</u>

The EF 2-3 peptide, with the sequence shown in **Figure 1B** and with the N-terminus acetylated and the C-terminus amidated, was purchased as a lyophilized powder (Biomatik USA, Wilmington, Delaware, USA).

b. Isothermal Titration Calorimetry (ITC)

Binding of lanthanides to EF 2-3 was determined by using a TA Instruments Affinity ITC system. All solutions were degassed for 10 min prior to the experiments and measurements were performed at 25 ˚C. The ITC cell contained 80 μM EF 2-3 in Chelex-treated 30 mM MOPS, 100 mM KCl, pH 7.4 and the titrant syringe contained 800 μM $LaCl_3$, $EuCl_3$, or $TbCl_3$ in the same buffer. Titration settings were the following: 125 rpm stirring speed, 180 s spacing between each injection, and 32 × 1.5 μL injections. In order to determine the heat of dilution, the same metal solution was titrated into an ITC cell containing a buffer blank. Although Tris has been reported to be a lesser interacting buffer than MOPS for lanthanide(III) ions,[24] we found that initial experiments in Tris exhibited large heats of dilution, so MOPS, in which heats of dilution were much smaller, was used instead. The heat of dilution was subtracted from the sample data set through the software and fitted using the "independent" ITC model to calculate the conditional dissociation constant (K_d) and stoichiometry (n). Uncertainties were determined from standard deviations from three independent titrations. ITC data analysis was conducted using TA Instrument's NanoAnalyze software.

c. Circular Dichroism (CD) Spectroscopy

Circular dichroism (CD) spectra of EF 2-3 were collected at 25 ˚C using a Jasco J-1500 CD spectrometer with a 1-mm pathlength quartz CD cuvette (Jasco J/0556). Samples were scanned from 255 nm to 195 nm, with the following instrument settings: 1 nm bandwidth, 0.5 nm data pitch, 50 nm/min scan rate, and 4 s averaging time. The cuvette contained 40 μM EF 2-3 in 200 μL of Chelex-treated 20 mM Tris, 100 mM KCl, pH 7.4, and was titrated with up to 100 μM $LaCl_3$, $EuCl_3$, or $TbCl_3$ from a 4.0 mM solution in the same buffer. A buffer blank spectrum (without peptide) was subtracted from the sample spectra, and the molar ellipticity at 222 nm versus metal equivalent was plotted. Uncertainties were determined from standard deviations from two independent titrations.

d. Two-Dimensional Infrared Spectroscopy

A 100 mM MOPS buffer at pH 7.4 was used as a solvent for both the peptide and metal chloride solutions. The peptide concentration was 25 μM, and the metal chlorides, $LaCl_3$, $EuCl_3$, and $TbCl_3$, were at a concentration of 50 μM. Experimental 2D IR spectra were measured using a custom-built 2D IR spectrometer.[18] In brief, a pair of pump pulses induces frequency-selective excitation of the amide-I backbone and the carboxylate asymmetric stretching modes. The excitation is subsequently probed using a third "probe" pulse. The excitation frequency is computed through a numerical Fourier transformation of the time delay separating the two pump pulses. The probe and signal are then measured in the frequency domain using a grating spectrometer equipped with a 128×128-pixel mercury cadmium telluride (MCT) array. The 2D IR signal amplitude for each pump frequency, referred to as the pump-slice amplitude (PSA),[20] is plotted to generate a spectrum that can be interpreted similarly to an FTIR spectrum. The pump-probe waiting time for all 2D IR spectra was held constant at 150 fs. The population time between the two pumps was also held constant at 500 fs. Perpendicular geometry was used for the setting of pump and probe polarizations. Phase cycling was utilized via a pulse shaper to minimize contributions due to pump

scatter. An average of 5 million shots was measured for each spectrum, or approximately 90 min of data acquisition for each sample.

e. Computational Methods and Analysis Techniques

Simulations closely follow a previous protocol developed for full-length LanM.[19] In brief, simulations were carried out using a modified CHARMM36 force field for the peptide[22] and the TIP3P-CHARMM water model.[21] The initial coordinates for EF 2-3 were extracted from the NMR structure (PDB: 6MI5, structure 1).[6] The initial structure was energy minimized and then equilibrated in a box containing ~2500 water molecules. Sodium ions were also added to maintain charge neutrality within the simulation box. The lanthanide ions were modeled using recent lanthanide-specific force field parameters.[23] The production simulation ran for 100 ns at 300 K and 1 bar using the Nose-Hoover and Parrinello-Rahman thermostat and barostat respectively.[22, 25, 26] Monodentate and bidentate binding features were determined on the final trajectory obtained from MD simulation. The MD structural analysis classified each ligand as monodentate, bidentate, intermediate, or unbound, using a two-step classification protocol that was used on LanM previously.[19] First, the α-carbon to ion distance of each ligand was calculated, with a distance larger than 0.4 nm being classified as "unbound." Then, the difference in oxygen-to-ion distance was used to classify each ligand as monodentate (>0.15 nm), bidentate (0–0.05 nm), or intermediate (0.05–0.15 nm) as demonstrated in **Figure 1D**. Plots of binding populations are compared to populations measured in 2D IR spectra. For an organized list of the various simulations carried out, refer to **Section S.1** in the Supporting Information.

f. Eu^{3+} Luminescence Lifetime Determination

EF 2-3 was diluted to 40 μM with 1 equivalent of $EuCl_3$ in 20 mM Tris, 100 mM KCl, pH 7.4. To prepare samples dissolved in deuterated buffer, 1 mL of this solution was lyophilized overnight and then resuspended in an equal volume of D_2O. This process was repeated once more. Subsequently, samples of 40 μM EF 2-3 in H_2O and 40 μM in D_2O were mixed in ratios to achieve concentrations ranging from 0% to 75% D_2O. Lifetime measurements were acquired on a Horiba Fluorolog-QM fluorometer with the following parameters: excitation at 394 nm, emission at 617 nm, start time at 13 μs, and end time at 2500 μs. The $1/\boldsymbol{\tau}$ values were determined from fitting a single exponential decay to the data ranging from 195 μs to 2500 μs. Starting at 195 μs removed the large contribution from the incident beam. These values were plotted against the $\%H_2O$ to determine $1/\boldsymbol{\tau}$ in 100% D_2O from the y-intercept of the trendline. The q value was calculated using the method described by Horrocks (eq 1), where A = 1.11 ms for Eu, n_{OH} is the number of alcoholic O−H coordinated to the metal, n_{NH} is the number of amine N−H coordinated to the metal, and $n_{O=CNH}$ is the number of amide N−H in which amide carboxylic oxygens is coordinated to the metal.[27] We assume that EF 2-3 has no contributions of n_{OH} and n_{NH}, thus these values are set to zero. When the other equation described by Horrocks and Sudnick was used,[28, 29] it yielded a similar value (less than 5% difference). Uncertainties were determined from standard deviations from three independent experiments.

$$q = A(1/\boldsymbol{\tau}_{H2O} - 1/\boldsymbol{\tau}_{D2O} - 0.31 + 0.45n_{OH} + 0.99n_{NH} + 0.075n_{O=CNH}) \quad \text{(Eq 1)}$$

3. Results

a. Secondary structure analysis of EF 2-3 using circular dichroism spectroscopy

The LanM fragment EF 2-3 is 41 amino acids in length and comprises the metal-binding loop complex (from EF 2 to EF 3) with two additional amino acids flanking both the N- and C-termini of the peptide, from the wild-type LanM sequence (**Figure 1B**). Previous research involving isolated EF peptides (e.g., EF1) demonstrated a markedly decreased affinity (with dissociation constant, K_d, values around 8 μM) compared to the full-length LanM,[17] as well as ~5 coordinated water molecules, as opposed to the 2 coordinated water molecules present in LanM as observed by biochemical[15] and structural[7] studies. Therefore, the lanthanide-bound individual EF hand peptides bore little resemblance to the lanthanide-bound metal sites in LanM. On the other hand, the lanthanide binding tag (LBT), an engineered peptide derived from an EF hand of a calcium-binding protein and of similar length (20 amino acids long, including the N- and C-terminal extensions), exhibited a binding affinity for Tb of 19 nM, much tighter than the individual LanM EF hand peptides.[30, 31] The optimization process of the LBT showed that the hydrophobic core and extended N- and C-termini can increase the binding affinity. Thus, we hypothesized that EF 2-3 may be able to achieve higher binding affinity than the individual EF hands as it possesses an inherent hydrophobic core and has elongated N- and C-termini that may be able to form REE-dependent helical structure, as those residues do in the full-length LanM (**Figure 1B**).

First, changes in the secondary structure of EF 2-3 upon metal titration were tracked using CD spectroscopy. The molar ellipticity at 222 nm ($[\theta]_{222nm}$), which monitors alpha-helix formation, was found to be −70,000 deg cm^2 dmol^{-1} (mean residue ellipticity of −1,700 deg cm^2 dmol^{-1}) for apo EF 2-3 at pH 7.4 (**Figure 2**). Given that the full-length apo LanM at pH 7.2 has a $[\theta]_{222nm}$ value of −500,000 deg cm^2 dmol^{-1} (mean residue ellipticity of −4,500 deg cm^2 dmol^{-1}),[10] helical regions were minimal in the apo EF 2-3. The observed changes in $[\theta]_{222nm}$ were −39,400 ± 14,800, −32,900 ± 3,800, and −32,200 ± 4,800 deg cm^2 dmol^{-1} for La, Eu, and Tb, respectively, resulting in a molar ellipticity value of −110,000 deg cm^2 dmol^{-1} for holo EF 2-3 at saturation. The calculated mean residue ellipticity was −2,600 deg cm^2 dmol^{-1}, suggesting approximately 9% helical character based on a value of −30,000 deg cm^2 dmol^{-1} for a fully α-helical protein. By comparison, the mean residue ellipticity of full-length holo-LanM is −16,000 deg cm^2 dmol^{-1}, and the x-ray crystal structure of LanM exhibits ~39% helical character in the corresponding sequence of the EF 2-3 region (**Figure S1-S2**). Prediction of secondary structure using BeStSel[32] for EF 2-3 suggested that only ~4% helical content in contrast to full-length LanM, which has ~23% under pH 7.2 condition (**Figure 2D**). We note that BeStSel appears to underestimate helical content and overestimates beta strand content evident from NMR[6] and crystallographic[7] characterization of LanM. Overall, this analysis suggests that the EF 2-3 peptide does not undergo the same conformational changes as LanM.

Regardless of the ion, the helical content of EF 2-3 demonstrates saturation with one equivalent metal binding (**Figure 2**). Similar saturation behavior was also observed in the ~200 nm region, where metal ion addition decreased the magnitude of the ellipticity, suggestive of ordering of regions of the peptide that are random coil in the apo form (**Figure S3**). These data suggest either that only one of the two metal binding sites of EF 2-3 is occupied, or no further conformational changes visible by CD occur after one equivalent binding.

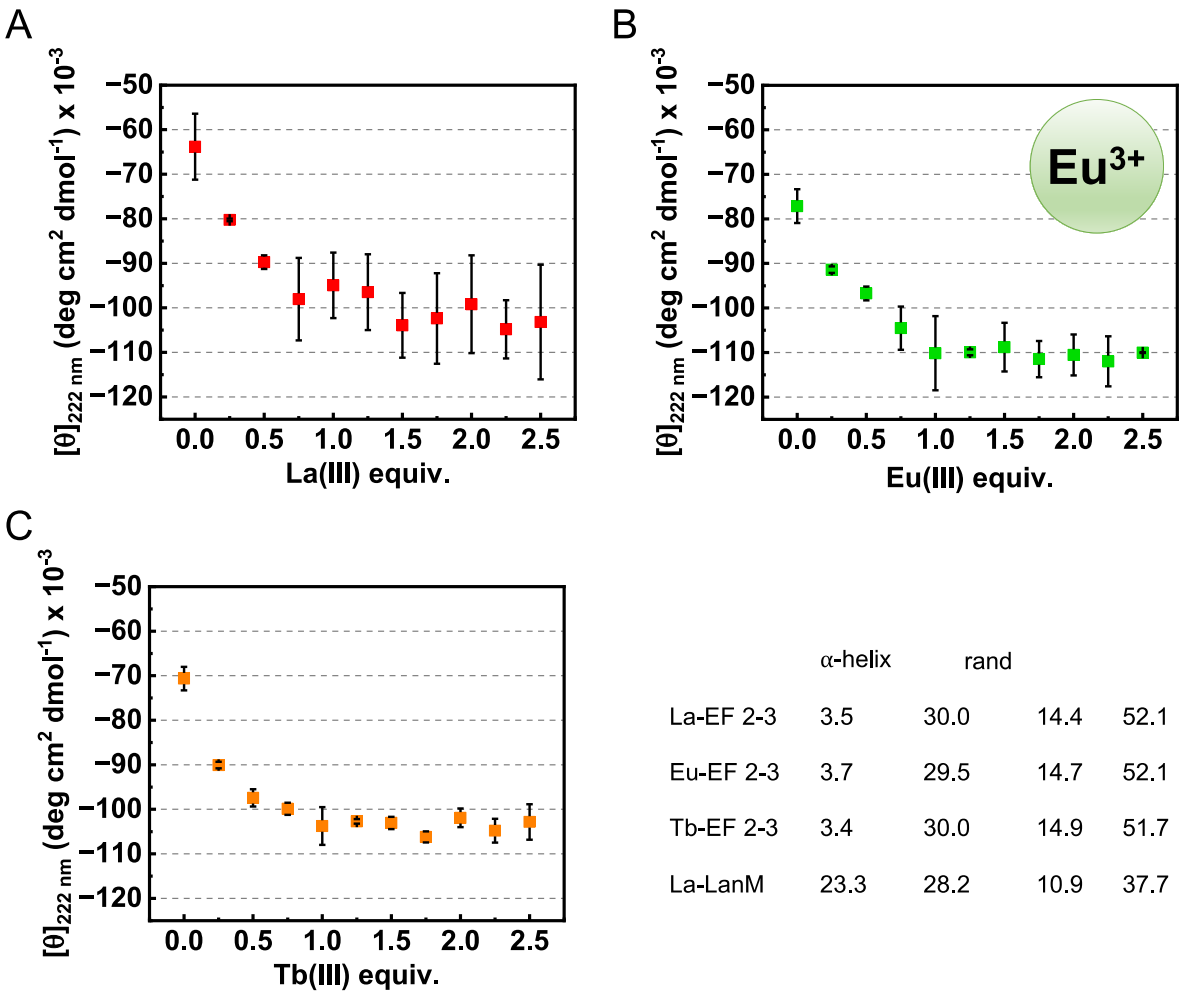

	α-helix		rand	
La-EF 2-3	3.5	30.0	14.4	52.1
Eu-EF 2-3	3.7	29.5	14.7	52.1
Tb-EF 2-3	3.4	30.0	14.9	51.7
La-LanM	23.3	28.2	10.9	37.7

Figure 2. Metal binding stoichiometry assessed by CD spectroscopy. A solution of 40 μM EF 2-3 was titrated with lanthanide ions at pH 7.4. Molar ellipticity [θ] at 222 nm obtained from CD spectra was plotted against 0–2.5 equivalents of (A) La^{3+}, (B) Eu^{3+}, and (C) Tb^{3+}. (D) The predicted secondary structure content of EF 2-3 was generated using BeStSel, based on the CD results. The CD data for La^{3+}-bound LanM were obtained at pH 7.2.

b. Isothermal titration calorimetry supports a single higher-affinity site in EF 2-3

Table 1. Conditional dissociation constants (K_d) and binding stoichiometry (n) of 80 μM EF 2-3 titrated with lanthanides and monitored using ITC. As the potential for weak interactions between the lanthanide ions and the buffer was not explicitly calculated herein, the K_d values are termed conditional. Conditions: 30 mM MOPS, 100 mM KCl, pH 7.4, 25˚C.

Ion	K_d (μM)	n
La^{3+}	25 ± 12	1.2 ± 0.1
Eu^{3+}	24 ± 8	1.2 ± 0.2
Tb^{3+}	23 ± 6	1.3 ± 0.1

The CD response of EF 2-3 to ~1 equivalent of La^{3+}, Eu^{3+}, and Tb^{3+} under the conditions of **Figure 2** suggested a binding event with $K_d < 40$ μM. Isothermal titration calorimetry was used to obtain more detailed information regarding the EF 2-3 binding affinities. The thermograms revealed that the complexation of EF 2-3 with La^{3+}, Eu^{3+}, and Tb^{3+} is endothermic (**Figure S2**). The endothermic response was also observed previously with individual EF peptides[17]; this is in contrast to metal binding to the full-length protein.[10, 33] In the case of EF 2-3, the enthalpies did not reach zero upon titration of 3 or even 5 equivalents of metal ion, although the bulk of the reaction had occurred within 3 equivalents especially in the case of La (**Figure S4**). As discussed in the legend of **Figure S4** we interpret this result as reflecting weak binding interactions underlying a primary, stronger interaction; this interpretation is also consistent with the CD data that suggest only one equivalent of binding leads to a significant conformational change. Therefore, we truncated the data after addition of 3 equivalents for sake of analysis. With the caveat that underlying weak interactions may impact the quantification, the fitted data did not reveal significant variations for different ions. At pH 7.4, the conditional dissociation constants (K_d) of EF 2-3 for La^{3+}, Eu^{3+}, and Tb^{3+} were found to be 25 μM, 24 μM, and 23 μM**,** respectively (**Table 1**). In all three cases, the ΔH values were small but binding was associated with rather large, positive ΔS values, perhaps related to release of water upon metal binding to the peptide (**Table S2**). Furthermore, the binding affinities of EF 2-3 were observed to be six orders of magnitude lower than those of the full-length LanM, as determined at pH 7.2.[10]

The binding stoichiometry (n), also measured using ITC, showed a stoichiometry of ~1 for the interactions between all three metal ions and EF 2-3 (**Table 1**). This suggests that only one of the two available sites on EF 2-3 interacts with metal ions most strongly; as noted above, any additional interactions are much weaker. The single-ion (~1:1) binding correlation is consistent with findings from other measurements, including CD spectroscopy, 2D-IR, and MD simulations as described below.

c. Ln^{3+} Binding Populations using 2D IR Spectroscopy

The carboxylate coordination geometries of EF 2-3 were measured for the three ions La^{3+}, Eu^{3+}, and Tb^{3+}. Spectra were measured in the 1530 cm^{-1} to 1660 cm^{-1} region corresponding to the asymmetric carboxylate stretching band. The pump-slice amplitude (PSA) analysis method[20] provides line shapes that are analogous to FT IR but with the high signal-to-noise and absence of background inherent to 2D IR spectroscopy.[18]

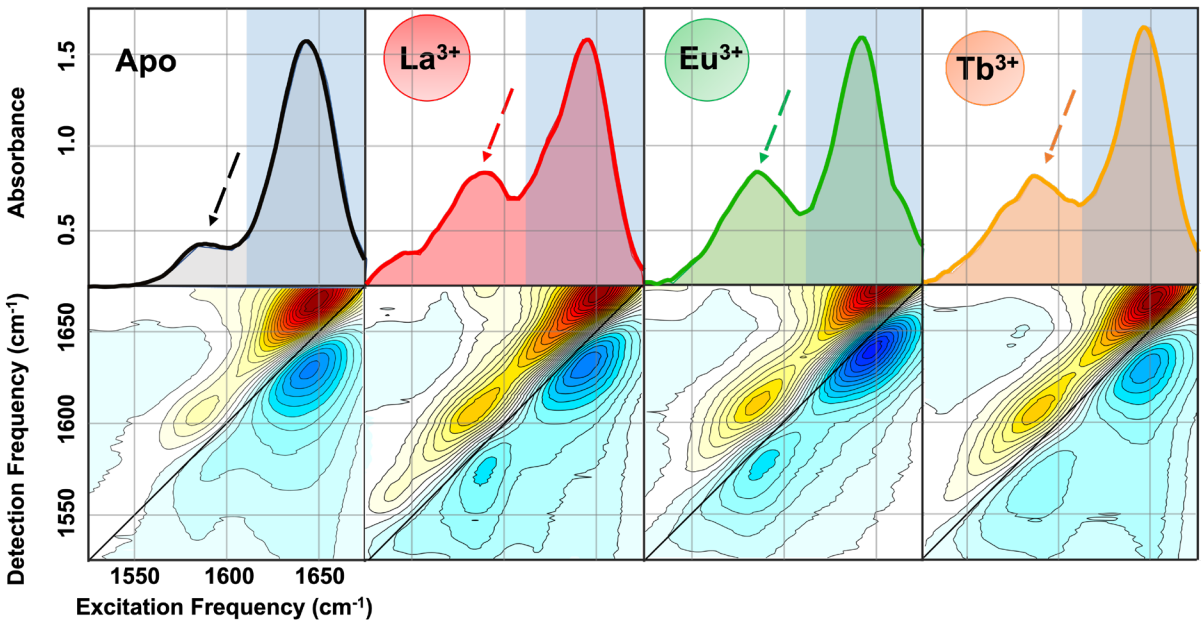

Figure 3. Measured 2D IR spectra with corresponding pump slice amplitude plots of EF 2-3, apo and complexed with the three lanthanide ions as indicated in each panel. Bidentate binding features appear around 1520-1550 cm^{-1}, unbound carboxylate features appear around 1580-1590 cm^{-1} (indicated by the dashed arrows), and monodentate binding features are observed around 1600-1620 cm^{-1}. The amide I band, centered at 1630 cm^{-1}, shown in front of the blue background is not analyzed in this study.

The 2D IR spectra of 25 μM EF 2-3 peptide reveal marked differences in the carboxylate asymmetric stretch region, ~1530-1620 cm^{-1}, between the apo peptide and the peptide in the presence of different metal ions at 50 μM (**Figure 3**). Qualitatively, the apo spectrum is compared to the spectra of the metal-bound peptide to observe differences between populations of different binding configurations. With the addition of La^{3+}, three partially overlapped peaks centered at 1540, 1590, and 1610 cm^{-1}, are observed. The features are deconvoluted by subtracting the apo features and the amide band (Supporting Information, section **S.4**). Together, these features give rise to a broad band spanning the 1530-1620 cm^{-1} region. Previous literature presents wavenumber ranges for the various carboxylate features to expect in the asymmetric region.[18-20] The spectral range from 1540 to 1570 cm^{-1} is indicative of carboxylate groups coordinating to metal ions in a bidentate manner. Therefore, in the analysis, the bidentate feature is fitted in this spectral region. The unbound carboxylate feature emerges in the spectral range 1570 to 1610 cm^{-1} and the monodentate feature emerges in the spectral range 1600-1610 cm^{-1}. Again, the spectral range for each feature is used to fit the features appropriately. EF 2-3 in the presence of Eu^{3+} and Tb^{3+} exhibits features that are slightly broader around 1590 cm^{-1} which can be attributed to overlapped bidentate and unbound carboxylate configurations. In addition, both spectra show monodentate features.[18]

Table 2. Relative populations of bidentate, monodentate and unbound carboxylate features to total observable peak area for EF 2-3 extracted from experimental 2D IR measurements. The populations are measured as the ratio of the individual peak amplitudes over total carboxylate band amplitude (Section S.4).

	La^{3+}	Eu^{3+}	Tb^{3+}
Bidentate	19.8 ± 3.3	29.4 ± 2.4	40.9 ± 2.2
Unbound	65.7 ± 1.4	58.6 ± 1.2	51.9 ± 4.1
Monodentate	14.5 ± 2.2	12.0 ± 1.5	7.2 ± 1.5

With the understanding of the spectral regions in which certain vibrational features emerge, we can quantify the relative populations of each feature to total observable band area by fitting the carboxylate band as a semi-quantitative metric of the relative populations of the different binding configurations (**Table 2**). All three lanthanides give rise to a mixed binding mode, encompassing both bidentate and monodentate binding, with a predominance of bidentate binding. We also observe 50-65% unbound features. The unbound carboxylates reflect the following contributions: 1) out of the 12 carboxylate residues in the EF 2-3 peptide, two are outside of the EF hands and not expected to contribute to metal binding; 2) the observations made in the ITC and CD measurements suggesting the peptide binds one equivalent of metal ions with highest affinity (**Table 1** and **Figure 2**); and 3) given K_d values of ~25 μM, the metal binding sites will only be partially occupied under the experimental conditions. The spectra also suggest that the population of bidentate carboxylates increases with the heavier lanthanide ions. This is in contrast to what is traditional observed for small chelators such as ethylenediaminetetraacetic acid (EDTA)[34, 35] and diethylenetriamine pentaacetate (DTPA)[36], perhaps due to the greater flexibility of the peptide relative to the small-molecule chelators. In summary, both monodentate and bidentate modes contribute to binding, but smaller ions contain larger proportions of bidentate populations stemming from stronger electrostatic interactions accommodated by the peptide structure.

d. Water-Lanthanide Competition using MD Simulations

MD simulations provide a molecular view of the experimentally measured bound conformation ensembles, giving a more detailed picture of the effects of the effect of ionic radius on the carboxylate conformations. Lanthanide-ion binding interactions are primarily driven by electrostatics;[22, 23, 25, 26] for this reason, the difference in ionic radii is used to describe the metal ion-carboxylate interactions between early and late lanthanides. Three ions were simulated: La^{3+}, Eu^{3+}, and Tb^{3+}.[23] The initial coordinates and structure for EF 2-3 were extracted from the NMR structure of the Y(III)-bound LanM. In addition, soft position restraints were placed on the alpha carbon backbone of the peptide to preserve the overall structure of the peptide but allow reorganization of the side chains. The MD simulations include only one lanthanide in either EF 2 or EF 3 to match the results obtained from CD and ITC that one of the two available sites on EF 2-3 interacts with metal ions (MD Simulation Key found in Table S1). As there is uncertainty with regards to which site is bound, simulations were done with either of the two sites bound. The results described below were carried out with one lanthanide present at the EF 2 site; however, similar populations were observed with the lanthanide present in the EF 3 binding site (**Figure S10**), and the interpretation would be the same for either site.

Following the structural analysis described previously, each ligand is classified as monodentate, bidentate, intermediate, or unbound as shown in **Figure 4**. This analysis leads to several important observations. First, all three lanthanides explored have a higher bidentate than monodentate binding population. Second, in comparing the bidentate binding population between the three lanthanides explored, this population increases with smaller ionic radius across the lanthanide series. These trends are in qualitative agreement with 2D IR spectra (**Table 2**). Lastly, the monodentate binding population decreases, albeit by small amounts, across the lanthanide series also in agreement with the populations extracted from 2D IR spectra.

MD simulations allow insight into parameters that are difficult to experimentally access, like characterizing binding geometries such as the bidentate configuration. Through MD, we can extract an estimate of binding populations. While numerical comparison is difficult, when MD is compared with spectra, we observe similar patterns to the experiment. In addition, when comparing the binding populations of EF 2-3 to previously reported populations for LanM through similar MD analysis,[19] we notice that greater populations of bidentate binding relative to monodentate binding are observed in both the EF 2-3 and the full protein, also supported by the x-ray structure of LanM.[7] Similarly, both systems display monodentate features as well; however, the change in populations between lanthanides is minimal, leading us to believe that the monodentate population may be largely independent of metal ion.

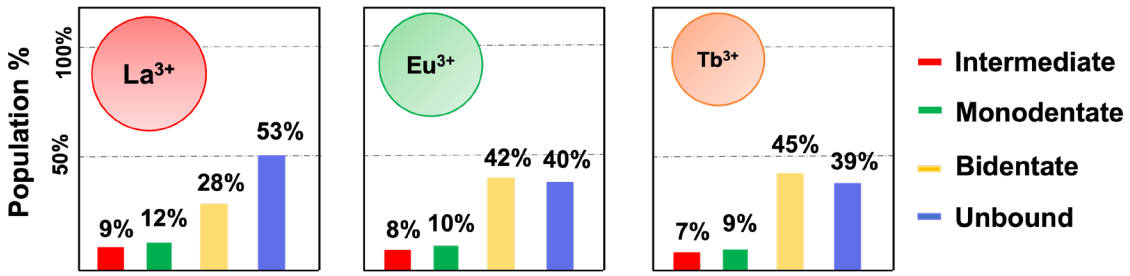

Figure 4. Carboxylate binding population analysis for EF 2-3 with La^{3+}, Eu^{3+}, and Tb^{3+} derived from MD simulations. There is a greater bidentate binding population than monodentate with decreasing ion size across the lanthanide series. The bidentate binding population increases and the monodentate binding population remains relatively unchanged; see Supporting Information, section S4.

In addition, canonical EF-hands, exemplified by CaM, typically contain water molecules directly coordinated to the ion.[18, 19] Therefore, it is imperative to study water-lanthanide interactions without imposing any a priori restrictions on simulations. Full-length *M. extorquens* LanM features two water molecules directly coordinating the metal ion and hydrogen bonding to metal-ligating carboxylates.[7, 15] Consequently, we also quantified the number of coordinating water molecules from the simulation trajectories.

While the primary focus of this study centers around EF 2-3, a comparison with its constituent parts, EF 2 and EF 3, allows us to discern any emergent properties or behaviors when these motifs are combined, and to understand the cooperative or antagonistic interactions that may arise when they function as an integrated unit. Therefore, populations of water molecules within a 0.3 nm radius[19] of the metal ion were assessed for simulations of EF 2-3 as well as for the individual EF 2 and EF 3 peptides (**Table 3**). The results for the EF 2 and EF 3 peptides corroborate previous experimental and computational results[17]; with ~5 coordinated water molecules, the metal sites of these peptides must bear little resemblance to the sites in the full protein. By contrast, the EF 2-3 peptide simulations reveal significantly fewer coordinated water molecules, closer to the 2

water molecules observed in experimental studies of the Nd^{3+}, Eu^{3+}, and Tb^{3+} complexes of LanM. In addition, the individual EF 2 and EF 3 peptide simulations suggest a greater unbound carboxylate population (around 70%; Supporting Information, Section S.9) than in EF 2-3 (around 50%). This result is consistent with the expectation that fewer carboxylate ligands would correlate with greater water coordination.

Table 3. Populations of water molecules within 0.3 nm of the metal ion within each binding site for EF 2, EF 3, and EF 2-3. This number is an average of water molecules around lanthanide ions observed over the trajectory of the simulation. We observe the individual motifs – EF 2 and EF 3 – have 4-5 molecules coordinated to the lanthanide ion present in the simulation. EF 2-3, on the other hand, has 2-3 molecules coordinated to the lanthanide ion in the simulation. In this simulation, the lanthanide ion was placed near EF 2. Simulation results for the water coordination when the lanthanide ion was placed near EF 3 can be found in Supporting Information, Section S.6. These values align with our experimental results discussed in Section 3.e.

	EF 2	EF 3	EF 2-3
La^{3+}	4.74	5.11	3.59
Eu^{3+}	4.88	5.27	2.52
Tb^{3+}	5.06	5.41	2.48

Considering that the trends in our experiments and MD simulations are in agreement, MD simulations of EF 2-3 with 2 Eu^{3+} ions present were run as a hypothetical state to further explore water-lanthanide and carboxylate-lanthanide competition. The goal was to observe if the presence of two ions alters the binding geometry for either of the two sites, compared to the single ion geometries. The results are shown in **Figure 5**. Here, there is a general "inverse" relationship between the water coordination at each site and the trend in bound carboxylate populations, suggesting that water and carboxylate remain in dynamic equilibrium that maintains the overall coordination number around the ion. This is also observed in Ln-ligand complexes containing carboxylates like DTPA.[36] Furthermore, there is dynamical heterogeneity that is observed in the MD simulations, and observations demonstrate that EF 2-3 does not behave similarly outside of the protein domain. In addition, it provides further support to our structural hypothesis that the cooperativity that exists between EF 2 and EF 3 in the full-length LanM does not persist when the EF 2-3 motif is observed independently.

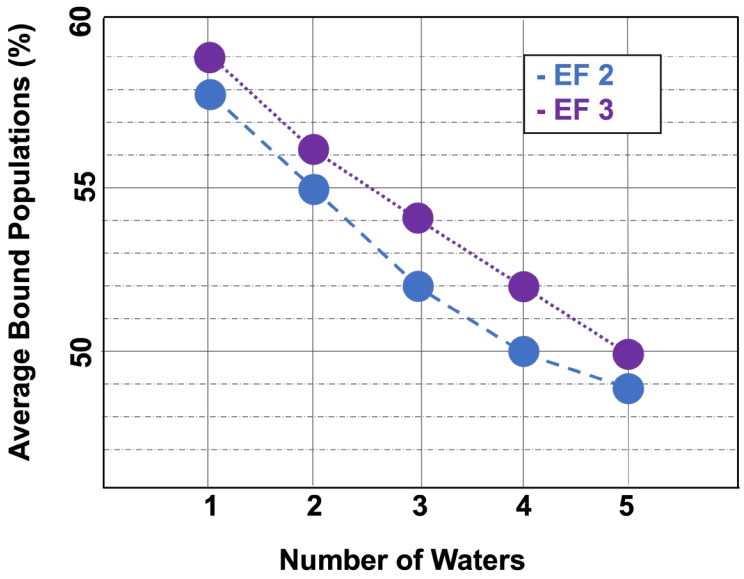

Figure 5. MD population analysis for EF 2-3 with two lanthanides (Eu^{3+} for the above results). Fewer coordinated water molecules corresponds to a larger carboxylate-bound population, indicating that there is a greater number of carboxylate groups of EF 2-3 coordinated to the lanthanide ion.

e. Investigation of coordinated solvent molecules using Eu luminescence lifetimes

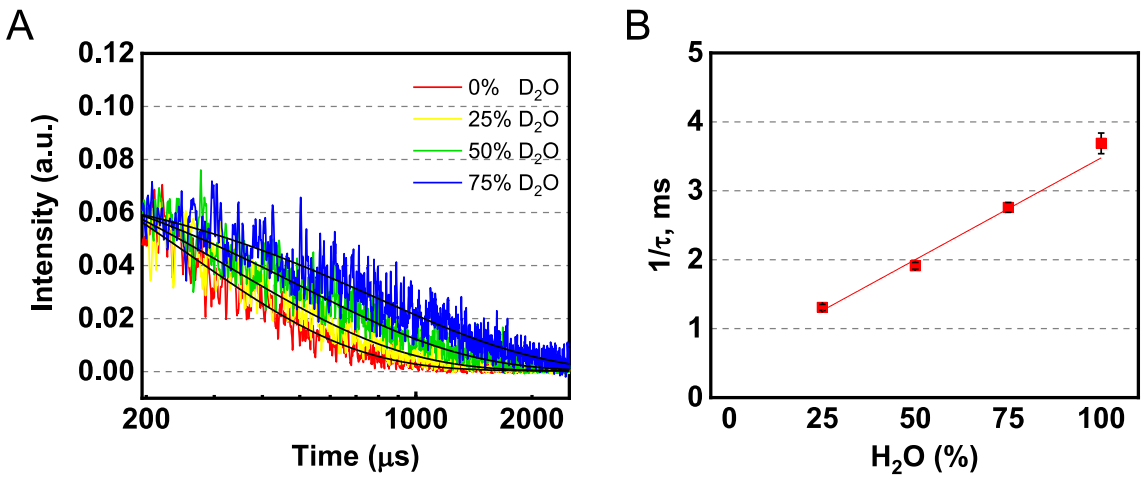

Figure 6. (A) Luminescence lifetime decay spectra of 40 µM Eu bound to 40 µM EF 2-3 in varying D_2O ratios at pH 7.4. Curves were fitted to a single exponential decay to determine $1/\tau$ values. (B) A plot of $1/\tau$ versus $\%H_2O$ with the equation of trendline and R^2 value.

Finally, we sought to experimentally test the MD prediction that the metal ions coordinated to the EF 2-3 peptide possessed ~3 coordinated water molecules. The number of water molecules (q) in the first coordination sphere of an Eu^{3+} ion is empirically correlated with the luminescence lifetime (τ) of the Eu^{3+} ion. The q value can be determined using a method which employs the difference in the decay constants (τ^{-1}) of Eu in H_2O and D_2O.[44,45] The luminescence decay of Eu^{3+}-EF 2-3 and the decay constants (τ^{-1}) determined from a single exponential fitting are plotted versus % H_2O in **Figure 6**, from which q was calculated using Equation 1. The determined q value for Eu^{3+}-EF 2-3 is 3.2, in line with the MD simulation results.

4. Discussion

One of the most important questions arising from the recent advent of the field of lanthanide biochemistry and its applications is the molecular origins of the high affinity and selectivity of Nature's ligands for these elements. LanMs, as the first and most extensively studied physiological, reversible chelators of the lanthanides, are an ideal model system in which to explore this complex question. A cellular ligand for lanthanides must have high affinity because of the propensity of lanthanide(III) ions to hydrolyze and pH values in the physiological regime and because of their low solubility in the presence of phosphate, which is abundant (tens of millimolar) inside cells. LanM is able to outcompete both of these reactions and bind lanthanides not just in the periplasm (its native localization) but also in the cytosol, as the LanM-based FRET sensor, LaMP1, responds to cytosolic lanthanides (La^{3+}, Ce^{3+}, Pr^{3+}, and Nd^{3+}) in *M. extorquens*.[37] LanM is also able to outcompete high concentrations of phosphate and other chelators in vitro,[38] although its affinity is insufficient in studies of radiolabeled LanM in a mouse tumor model.[10, 39]

Our investigation into the interaction of EF 2-3 with lanthanides has yielded several observations that shed light on how structure of the full-length LanM relates to achieving this high affinity, underpinned by a combination of techniques: ITC, CD, 2D IR, and MD simulations. The measurements point to a primary 1:1 metal:peptide binding stoichiometry with micromolar affinity, for the three examined ions. Whereas LanM preferentially binds early lanthanides, such selectivity was not evident in EF 2-3, underscoring the significance of the rest of the protein. Not only are the affinity and selectivity of peptides of individual EF hands[17] far from those of the full LanM (each EF hand's 12 residues being ~10% of the full-length protein); this is also the case for the EF 2-3 peptide that encompasses ~40% of the full-length protein. This observation argues even more strongly for the importance of the three core helices of the protein in dictating affinity and selectivity.[6, 10] Simultaneously, 2D IR spectroscopy, alongside MD simulations, examined the lanthanide binding modes of peptide carboxylates. Both 2D IR and MD simulations exhibit similar trends: both mono- and bidentate modes are evident across the ions, with smaller ions favoring the bidentate configurations. The binding populations extracted from 2D IR and MD simulations for EF 2-3 contrast those obtained for LanM, indicating that the EF 2-3 peptide behaves differently outside of the protein, likely reflecting an important role of the rest of the protein in constraining conformational plasticity of the EF 2-3 segment.[40, 41]

MD simulations shed further light on the dynamics of these interactions. In the present analysis of EF 2 and EF 3 trajectories, we observed partial coordination of the lanthanide ions by water, typically with an average of 4-5 molecules, far from the 2 observed for the metal sites of the full-length protein (**Table 3**). By contrast, the simulations for EF 2-3 show an average of only 2 to 3 water molecules interacting with the lanthanide ion, much closer to the observations in the full-length protein. The simulations are supported by experimental evidence for ~3 coordinated molecules for Eu^{3+} in the presence of EF 2-3 (**Figure 6**). Interestingly, while the binding affinity of EF 2-3 (K_d = 25 μM) is lower than that of individual EF hands (K_d = ~8 μM), the water coordination for EF 2-3 is lower (~3) than for the individual EF-hands (~5).[17] Studies of variants of the D_9 position of the EF hands in LanM have shown a similar counterintuitive lack of correlation between number of coordinated solvent molecules and apparent metal binding affinity.[16] Together, the observations with the EF 2, EF 3, and EF 2-3 peptides support the crystallographic picture of metal sites for which exactly two coordinated solvent molecules,

extensively hydrogen bonding to metal-ligating protein residues and to each other, are critical to the integrity of the sites.[7] Furthermore, our observations imply that the hydrophobic regions between EF 2 and EF 3 in EF 2-3, as well as the extended N- and C-termini, are not sufficient to enhance the binding affinity. Instead, they assist in arranging the binding loop to exclude water molecules in the first coordination sphere, perhaps to arrange a metal-binding site more similar in structure to those in the full-length protein. This information is valuable in understanding how LanM achieves high affinity for lanthanide ions with two water molecules coordinated. Potentially, our observations with EF 2-3 may reflect initial metal binding to the full-length protein; as soon as the alpha helices form, the binding loop is arranged to remove the third water molecule, achieving an optimized binding geometry for the metal ion with two water molecules still present.

There is still the question of why EF 2-3 only coordinates a single lanthanide ion with the highest affinity, whereas in the full protein, a metal ion is coordinated to each hand motif.[15] In the full LanM protein, EF hands 2 and 3 have the highest binding affinities.[14-16] Our results suggest that the cooperativity between these two EF hands in the full protein likely involves lanthanide binding to one EF hand inducing a conformational change in regions of the protein beyond the EF 2-3 unit – for example, the C-terminal helix that packs against EF 2/3 in the folded structure – which allows the other EF hand to bind a lanthanide. By contrast, when EF 2-3 is observed outside of the protein domain, only one EF hand binds well because this conformational change cannot occur without the extended protein scaffold. This proposed mechanism echoes allosteric binding phenomena observed in other proteins.[41]

Our observations are also intriguing in the context of other EF-hand proteins, the vast majority of which have physiological functions of calcium binding, for example extensively studied CaM. The N- and C-terminal lobes of CaM, each containing two EF hands, can be purified separately and studied, with similar binding affinities to the full-length protein.[42] By contrast, the same is clearly not true of the EF 2-3 peptide of LanM, which is the closest analog to a lobe of CaM. One of the distinguishing features of LanMs among EF-hand proteins – indeed one that allows identification of members of the LanM protein family by sequence alone[7] – is the shorter spacing between adjacent EF hand loops, 12-13 residues instead of the typical 24-25 residues in canonical EF-hand proteins.[10, 43] Upon solution of the NMR structure of the Y^{3+}-bound protein, we hypothesized that the short helices comprising these inter-loop residues in LanM served to poise the protein between order and disorder.[6] Characterization of the EF 2-3 peptide in the present work strongly supports this hypothesis. Even when saturated with lanthanide(III) ions, the peptide exhibits little helical content (**Figure 2D**), even less than the corresponding part of the full-length LanM structure. Furthermore, as mentioned above, the CD, ITC, and MD simulations support the notion that only one binding site retains significant affinity for lanthanides (though still much less than in the full-length protein). This situation contrasts with the two lobes of CaM, which retain the majority of their helical content even in the apo state and retain their ability to bind two equivalents of Ca^{2+}.[42, 44] This underscores our observations with each of our experimental methods that even 40% of the full-length LanM is insufficient to recapitulate – and, in fact, quite far from recapitulating – the properties of the same region within the intact protein. While it was perhaps not surprising that individual 12-residue EF hand peptides would be unable to capture the high affinity of the full-length protein, the failure of EF 2-3 to also do so speaks all the more strongly to the importance of the core helical bundle of the protein to constrain the conformational flexibility of the EF 2-3 domain to impart it with its high lanthanide affinity and selectivity.

5. Conclusions and Outlook

Our study has delved into the structural and lanthanide binding dynamics of the LanM peptide fragment, EF 2-3. Combining thermodynamic measurements with spectroscopy and MD simulations, this study has advanced our understanding of lanthanide-peptide interactions and emphasized the nuanced role of molecular structures in providing details that complement experimental work. The study accentuates the importance of structure in dictating function; it highlights ways in which the isolated EF 2-3 unit behaves similarly and ways it behaves distinctly from its integrated role within the full-length LanM protein. Cooperativity in the full LanM protein is lost or diminished in the isolated EF 2-3 domain. Coupled with this, our observations of the water-lanthanide and carboxylate-lanthanide coordination competition suggests a nuanced equilibrium between the peptide's local environment and its binding affinity.

Finally, within the context of lanthanide separations, current technologies predominantly employ small organic ligands, positioning LanM as an eco-friendly alternative. However, our work shows that the task of designing smaller peptide-centric chelators – even those closely based on existing ligands like LanM – poses additional complexities. Recognizing and accounting for these intricacies will be paramount in furthering the development of sustainable separation and purification methods. This is true not merely for lanthanides but also for other technology metals, as strategies for metal recovery and separation that integrate native and engineered biological machineries are becoming an increasingly explored direction of chemical biology.

Supporting Information

CD spectra and ITC thermograms, further details on Pump Slice Amplitude analysis and spectral fitting, binding configurations, and water coordination analysis for EF 2-3; population analysis of MD simulations for EF 2 and EF 3.

Acknowledgements

This work was supported by the Welch Foundation (F-1891 to C.R.B.), the National Institutes of Health (R35GM133359 to C.R.B.), the National Science Foundation (CHE-1945015 to J.A.C.) and the Alfred P. Sloan Foundation (to J.A.C.). Simulations were carried out using the Texas Advanced Computing Center (TACC) Lonestar6 cluster.

References

(1) Firsching, F. H.; Brune, S. N. Solubility products of the trivalent rare-earth phosphates. *Journal of Chemical & Engineering Data* **1991**, *36* (1), 93-95. DOI: 10.1021/je00001a028.
(2) Arshi, P. S.; Vahidi, E.; Zhao, F. Behind the Scenes of Clean Energy: The Environmental Footprint of Rare Earth Products. *ACS Sustainable Chemistry & Engineering* **2018**, *6* (3), 3311-3320. DOI: 10.1021/acssuschemeng.7b03484.
(3) Cheisson, T.; Schelter, E. J. Rare earth elements: Mendeleev's bane, modern marvels. *Science* **2019**, *363* (6426), 489-493. DOI: doi:10.1126/science.aau7628.

(4) Cotruvo, J. A., Jr. The Chemistry of Lanthanides in Biology: Recent Discoveries, Emerging Principles, and Technological Applications. *ACS Central Science* **2019**, *5* (9), 1496-1506. DOI: 10.1021/acscentsci.9b00642.
(5) Xie, F.; Zhang, T. A.; Dreisinger, D.; Doyle, F. A critical review on solvent extraction of rare earths from aqueous solutions. *Minerals Engineering* **2014**, *56*, 10-28. DOI: https://doi.org/10.1016/j.mineng.2013.10.021.
(6) Cook, E. C.; Featherston, E. R.; Showalter, S. A.; Cotruvo, J. A., Jr. Structural Basis for Rare Earth Element Recognition by Methylobacterium extorquens Lanmodulin. *Biochemistry* **2019**, *58* (2), 120-125. DOI: 10.1021/acs.biochem.8b01019.
(7) Mattocks, J. A.; Jung, J. J.; Lin, C.-Y.; Dong, Z.; Yennawar, N. H.; Featherston, E. R.; Kang-Yun, C. S.; Hamilton, T. A.; Park, D. M.; Boal, A. K.; Cotruvo, J. A. Enhanced rare-earth separation with a metal-sensitive lanmodulin dimer. *Nature* **2023**, *618* (7963), 87-93. DOI: 10.1038/s41586-023-05945-5.
(8) Fitriyanto, N. A.; Fushimi, M.; Matsunaga, M.; Pertiwiningrum, A.; Iwama, T.; Kawai, K. Molecular structure and gene analysis of Ce3+-induced methanol dehydrogenase of Bradyrhizobium sp. MAFF211645. *Journal of Bioscience and Bioengineering* **2011**, *111* (6), 613-617. DOI: https://doi.org/10.1016/j.jbiosc.2011.01.015.
(9) Hibi, Y.; Asai, K.; Arafuka, H.; Hamajima, M.; Iwama, T.; Kawai, K. Molecular structure of La3+-induced methanol dehydrogenase-like protein in Methylobacterium radiotolerans. *Journal of Bioscience and Bioengineering* **2011**, *111* (5), 547-549. DOI: https://doi.org/10.1016/j.jbiosc.2010.12.017.
(10) Cotruvo, J. A., Jr.; Featherston, E. R.; Mattocks, J. A.; Ho, J. V.; Laremore, T. N. Lanmodulin: A Highly Selective Lanthanide-Binding Protein from a Lanthanide-Utilizing Bacterium. *Journal of the American Chemical Society* **2018**, *140* (44), 15056-15061. DOI: 10.1021/jacs.8b09842.
(11) Nitz, M.; Sherawat, M.; Franz, K. J.; Peisach, E.; Allen, K. N.; Imperiali, B. Structural Origin of the High Affinity of a Chemically Evolved Lanthanide-Binding Peptide. *Angewandte Chemie International Edition* **2004**, *43* (28), 3682-3685. DOI: https://doi.org/10.1002/anie.200460028.
(12) Deblonde, G. J. P.; Mattocks, J. A.; Park, D. M.; Reed, D. W.; Cotruvo, J. A., Jr.; Jiao, Y. Selective and Efficient Biomacromolecular Extraction of Rare-Earth Elements using Lanmodulin. *Inorganic Chemistry* **2020**, *59* (17), 11855-11867. DOI: 10.1021/acs.inorgchem.0c01303.
(13) Dong, Z.; Mattocks, J. A.; Deblonde, G. J. P.; Hu, D.; Jiao, Y.; Cotruvo, J. A., Jr.; Park, D. M. Bridging Hydrometallurgy and Biochemistry: A Protein-Based Process for Recovery and Separation of Rare Earth Elements. *ACS Central Science* **2021**, *7* (11), 1798-1808. DOI: 10.1021/acscentsci.1c00724.
(14) Chattopadhyaya, R.; Meador, W. E.; Means, A. R.; Quiocho, F. A. Calmodulin structure refined at 1.7 Å resolution. *Journal of Molecular Biology* **1992**, *228* (4), 1177-1192. DOI: https://doi.org/10.1016/0022-2836(92)90324-D.
(15) Featherston, E. R.; Issertell, E. J.; Cotruvo, J. A., Jr. Probing Lanmodulin's Lanthanide Recognition via Sensitized Luminescence Yields a Platform for Quantification of Terbium in Acid Mine Drainage. *Journal of the American Chemical Society* **2021**, *143* (35), 14287-14299. DOI: 10.1021/jacs.1c06360.
(16) Mattocks, J. A.; Cotruvo, J. A.; Deblonde, G. J. P. Engineering lanmodulin's selectivity for actinides over lanthanides by controlling solvent coordination and second-sphere interactions.

Chemical Science **2022**, *13* (20), 6054-6066, 10.1039/D2SC01261H. DOI: 10.1039/D2SC01261H.
(17) Gutenthaler, S. M.; Tsushima, S.; Steudtner, R.; Gailer, M.; Hoffmann-Röder, A.; Drobot, B.; Daumann, L. J. Lanmodulin peptides – unravelling the binding of the EF-Hand loop sequences stripped from the structural corset. *Inorganic Chemistry Frontiers* **2022**, *9* (16), 4009-4021, 10.1039/D2QI00933A. DOI: 10.1039/D2QI00933A.
(18) Edington, S. C.; Gonzalez, A.; Middendorf, T. R.; Halling, D. B.; Aldrich, R. W.; Baiz, C. R. Coordination to lanthanide ions distorts binding site conformation in calmodulin. *Proceedings of the National Academy of Sciences* **2018**, *115* (14), E3126-E3134. DOI: doi:10.1073/pnas.1722042115.
(19) Liu, S.; Featherston, E. R.; Cotruvo, J. A.; Baiz, C. R. Lanthanide-dependent coordination interactions in lanmodulin: a 2D IR and molecular dynamics simulations study. *Physical Chemistry Chemical Physics* **2021**, *23* (38), 21690-21700, 10.1039/D1CP03628A. DOI: 10.1039/D1CP03628A.
(20) Valentine, M. L.; Al-Mualem, Z. A.; Baiz, C. R. Pump Slice Amplitudes: A Simple and Robust Method for Connecting Two-Dimensional Infrared and Fourier Transform Infrared Spectra. *The Journal of Physical Chemistry A* **2021**, *125* (29), 6498-6504. DOI: 10.1021/acs.jpca.1c04558.
(21) Mark, P.; Nilsson, L. Structure and Dynamics of the TIP3P, SPC, and SPC/E Water Models at 298 K. *The Journal of Physical Chemistry A* **2001**, *105* (43), 9954-9960. DOI: 10.1021/jp003020w.
(22) Abraham, M. J.; Murtola, T.; Schulz, R.; Páll, S.; Smith, J. C.; Hess, B.; Lindahl, E. GROMACS: High performance molecular simulations through multi-level parallelism from laptops to supercomputers. *SoftwareX* **2015**, *1-2*, 19-25. DOI: https://doi.org/10.1016/j.softx.2015.06.001.
(23) Migliorati, V.; Serva, A.; Terenzio, F. M.; D'Angelo, P. Development of Lennard-Jones and Buckingham Potentials for Lanthanoid Ions in Water. *Inorganic Chemistry* **2017**, *56* (11), 6214-6224. DOI: 10.1021/acs.inorgchem.7b00207.
(24) Mandal, P.; Kretzschmar, J.; Drobot, B. Not just a background: pH buffers do interact with lanthanide ions—a Europium(III) case study. *JBIC Journal of Biological Inorganic Chemistry* **2022**, *27* (2), 249-260. DOI: 10.1007/s00775-022-01930-x.
(25) Parrinello, M.; Rahman, A. Polymorphic transitions in single crystals: A new molecular dynamics method. *Journal of Applied Physics* **1981**, *52* (12), 7182-7190. DOI: 10.1063/1.328693 (acccessed 11/7/2023).
(26) Huang, J.; MacKerell Jr, A. D. CHARMM36 all-atom additive protein force field: Validation based on comparison to NMR data. *Journal of Computational Chemistry* **2013**, *34* (25), 2135-2145. DOI: https://doi.org/10.1002/jcc.23354.
(27) Supkowski, R. M.; Horrocks, W. D. On the determination of the number of water molecules, q, coordinated to europium(III) ions in solution from luminescence decay lifetimes. *Inorganica Chimica Acta* **2002**, *340*, 44-48. DOI: https://doi.org/10.1016/S0020-1693(02)01022-8.
(28) Horrocks, W. D., Jr.; Sudnick, D. R. Lanthanide ion probes of structure in biology. Laser-induced luminescence decay constants provide a direct measure of the number of metal-coordinated water molecules. *Journal of the American Chemical Society* **1979**, *101* (2), 334-340. DOI: 10.1021/ja00496a010.

(29) Horrocks, W. D., Jr.; Sudnick, D. R. Lanthanide ion luminescence probes of the structure of biological macromolecules. *Accounts of Chemical Research* **1981**, *14* (12), 384-392. DOI: 10.1021/ar00072a004.
(30) Franz, K. J.; Nitz, M.; Imperiali, B. Lanthanide-Binding Tags as Versatile Protein Coexpression Probes. *ChemBioChem* **2003**, *4* (4), 265-271. DOI: https://doi.org/10.1002/cbic.200390046.
(31) Martin, L. J.; Sculimbrene, B. R.; Nitz, M.; Imperiali, B. Rapid Combinatorial Screening of Peptide Libraries for the Selection of Lanthanide-Binding Tags (LBTs). *QSAR & Combinatorial Science* **2005**, *24* (10), 1149-1157. DOI: https://doi.org/10.1002/qsar.200540007.
(32) Micsonai, A.; Wien, F.; Kernya, L.; Lee, Y.-H.; Goto, Y.; Réfrégiers, M.; Kardos, J. Accurate secondary structure prediction and fold recognition for circular dichroism spectroscopy. *Proceedings of the National Academy of Sciences* **2015**, *112* (24), E3095-E3103. DOI: doi:10.1073/pnas.1500851112.
(33) Chen, J.; Shi, W.; Ren, Y.; Zhao, K.; Liu, Y.; Jia, B.; Zhao, L.; Li, M.; Liu, Y.; Su, J.; et al. Strong Protein Adhesives through Lanthanide-enhanced Structure Folding and Stack Density. *Angewandte Chemie International Edition* **2023**, *62* (43), e202304483. DOI: https://doi.org/10.1002/anie.202304483 (acccessed 2023/11/28).
(34) Durand, S.; Dognon, J.-P.; Guilbaud, P.; Rabbe, C.; Wipff, G. Lanthanide and alkaline-earth complexes of EDTA in water: a molecular dynamics study of structures and binding selectivities. *Journal of the Chemical Society, Perkin Transactions 2* **2000**, (4), 705-714, 10.1039/A908879B. DOI: 10.1039/A908879B.
(35) Mathur, J. N.; Thakur, P.; Dodge, C. J.; Francis, A. J.; Choppin, G. R. Coordination Modes in the Formation of the Ternary Am(III), Cm(III), and Eu(III) Complexes with EDTA and NTA: TRLFS, 13C NMR, EXAFS, and Thermodynamics of the Complexation. *Inorganic Chemistry* **2006**, *45* (20), 8026-8035. DOI: 10.1021/ic052166c.
(36) Summers, T. J.; O'Brien, R. D.; Sobrinho, J. A.; de Bettencourt-Dias, A.; Cantu, D. C. Structural Changes to the Gd-DTPA Complex at Varying Ligand Protonation State. *European Journal of Inorganic Chemistry* **2023**, *n/a* (n/a), e202300507. DOI: https://doi.org/10.1002/ejic.202300507 (acccessed 2024/02/12).
(37) Mattocks, J. A.; Ho, J. V.; Cotruvo, J. A., Jr. A Selective, Protein-Based Fluorescent Sensor with Picomolar Affinity for Rare Earth Elements. *Journal of the American Chemical Society* **2019**, *141* (7), 2857-2861. DOI: 10.1021/jacs.8b12155.
(38) Deblonde, G. J.-P.; Mattocks, J. A.; Dong, Z.; Wooddy, P. T.; Cotruvo, J. A.; Zavarin, M. Capturing an elusive but critical element: Natural protein enables actinium chemistry. *Science Advances* **2021**, *7* (43), eabk0273. DOI: doi:10.1126/sciadv.abk0273.
(39) Martin, K. E.; Mattocks, J. A.; Śmiłowicz, D.; Aluicio-Sarduy, E.; Whetter, J. N.; Engle, J. W.; Cotruvo, J. A.; Boros, E. Radiolabeling and in vivo evaluation of lanmodulin with biomedically relevant lanthanide isotopes. *RSC Chemical Biology* **2023**, *4* (6), 414-421, 10.1039/D3CB00020F. DOI: 10.1039/D3CB00020F.
(40) Perutz, M. F. Mechanisms of cooperativity and allosteric regulation in proteins. *Q Rev Biophys* **1989**, *22* (2), 139-237. DOI: 10.1017/s0033583500003826 From NLM.
(41) Ackers, G. K. Deciphering the Molecular Code of Hemoglobin Allostery. In *Advances in Protein Chemistry*, Di Cera, E. Ed.; Vol. 51; Academic Press, 1998; pp 185-253.
(42) Linse, S.; Helmersson, A.; Forsén, S. Calcium binding to calmodulin and its globular domains. *Journal of Biological Chemistry* **1991**, *266* (13), 8050-8054. DOI: https://doi.org/10.1016/S0021-9258(18)92938-8.

(43) Gifford, Jessica L.; Walsh, Michael P.; Vogel, Hans J. Structures and metal-ion-binding properties of the Ca2+-binding helix–loop–helix EF-hand motifs. *Biochemical Journal* **2007**, *405* (2), 199-221. DOI: 10.1042/bj20070255 (acccessed 11/7/2023).
(44) Maune, J. F.; Beckingham, K.; Martin, S. R.; Bayley, P. M. Circular dichroism studies on calcium binding to two series of calcium binding site mutants of Drosophila melanogaster calmodulin. *Biochemistry* **1992**, *31* (34), 7779-7786. DOI: 10.1021/bi00149a006.

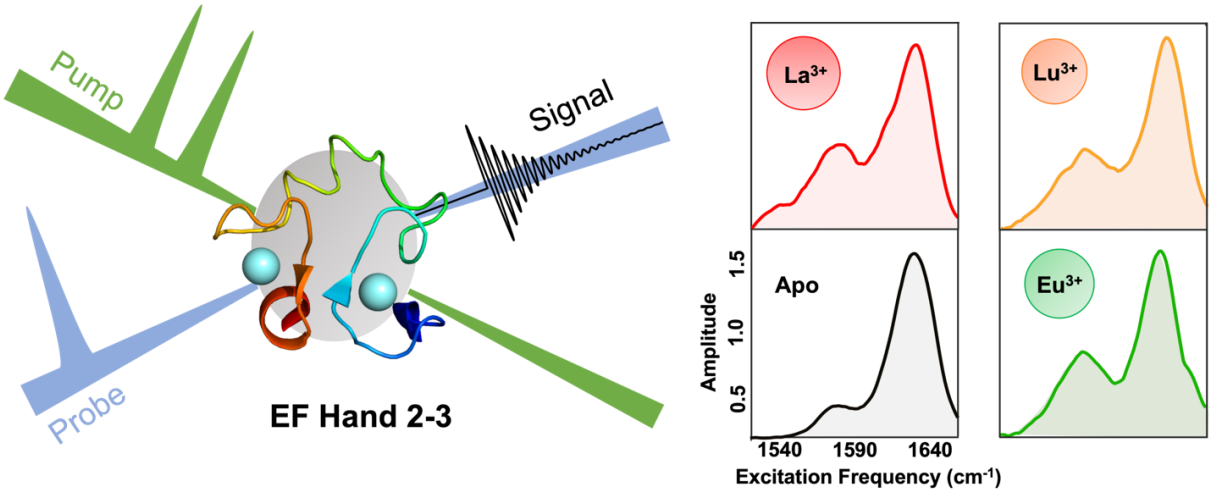
Pump
Signal
Probe
EF Hand 2-3
La3+
Lu3+
Apo
Eu3+
Amplitude
0.5
1.0
1.5
1540
1590
1640
Excitation Frequency (cm-1)

TOC Figure.